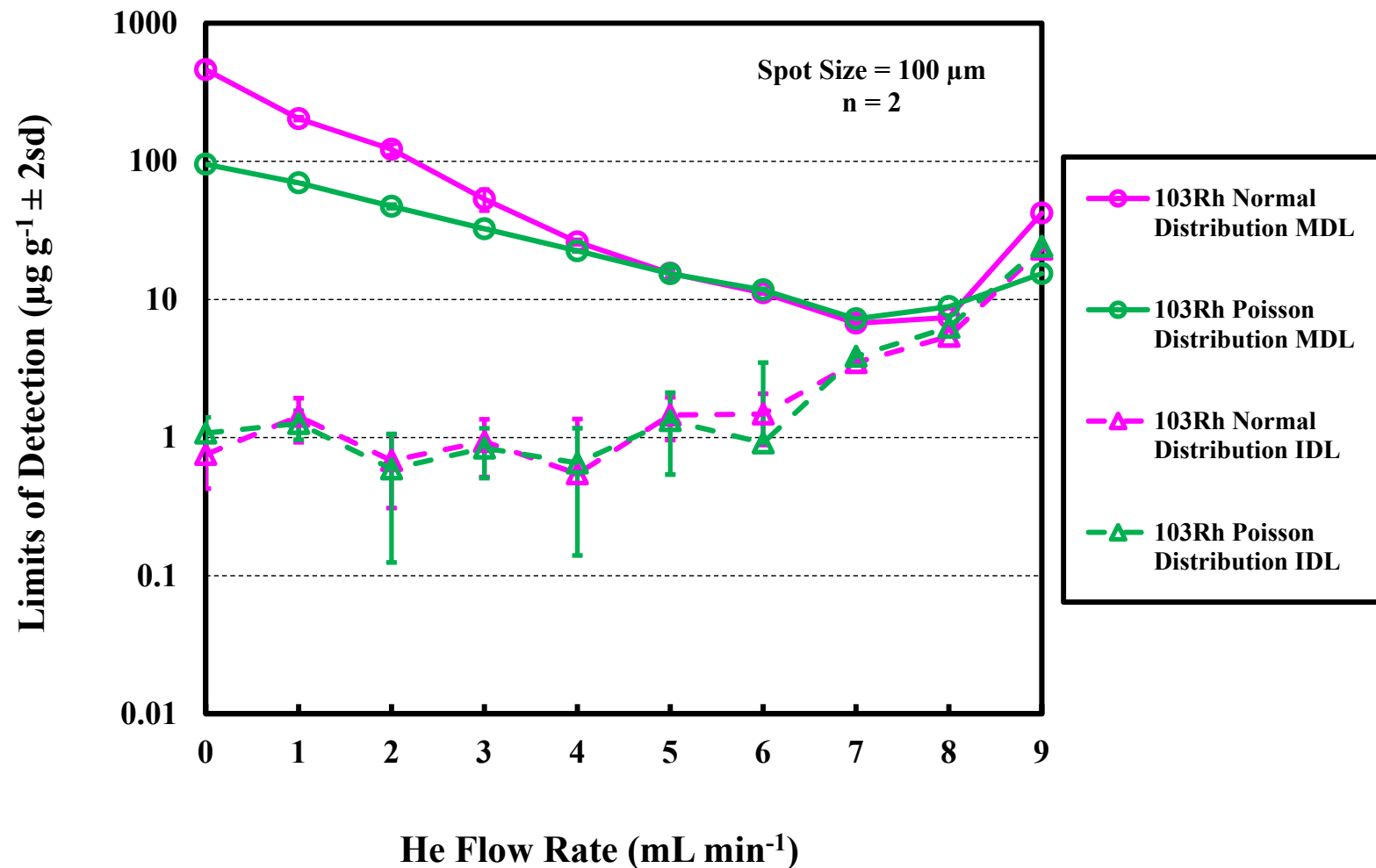


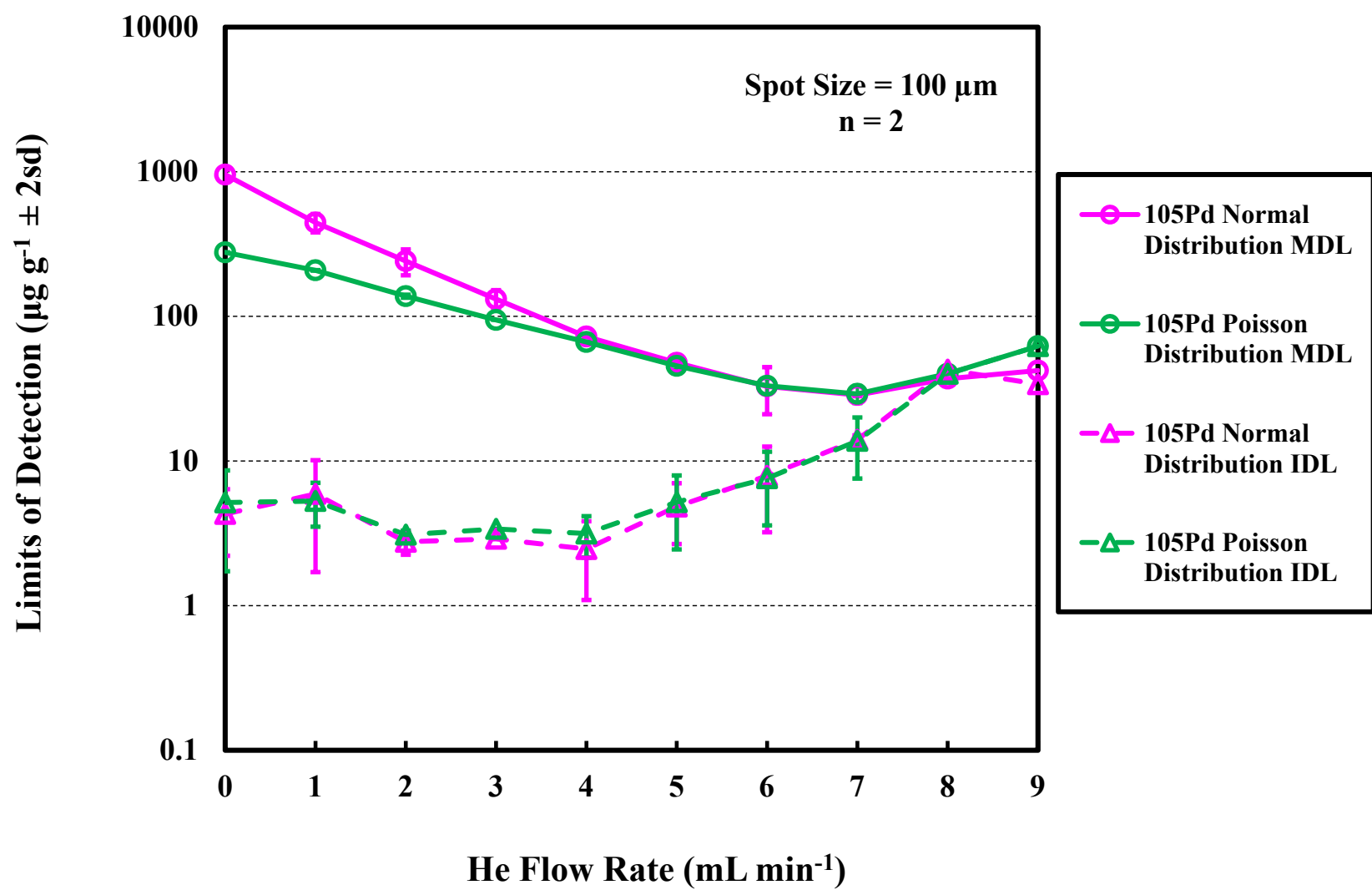
1

2 Supplementary Fig. 1† The instrument and method limits of detection (ILOD and MLOD) for ^{103}Rh and ^{105}Pd determined using the equations
3 of Longerich et al. (1996)⁶² and Pettke et al. (2012)⁶⁴ as a function of the total measured counts for Agilent 7700x LA-ICP-MS analysis of
4 chalcopyrite and bornite.



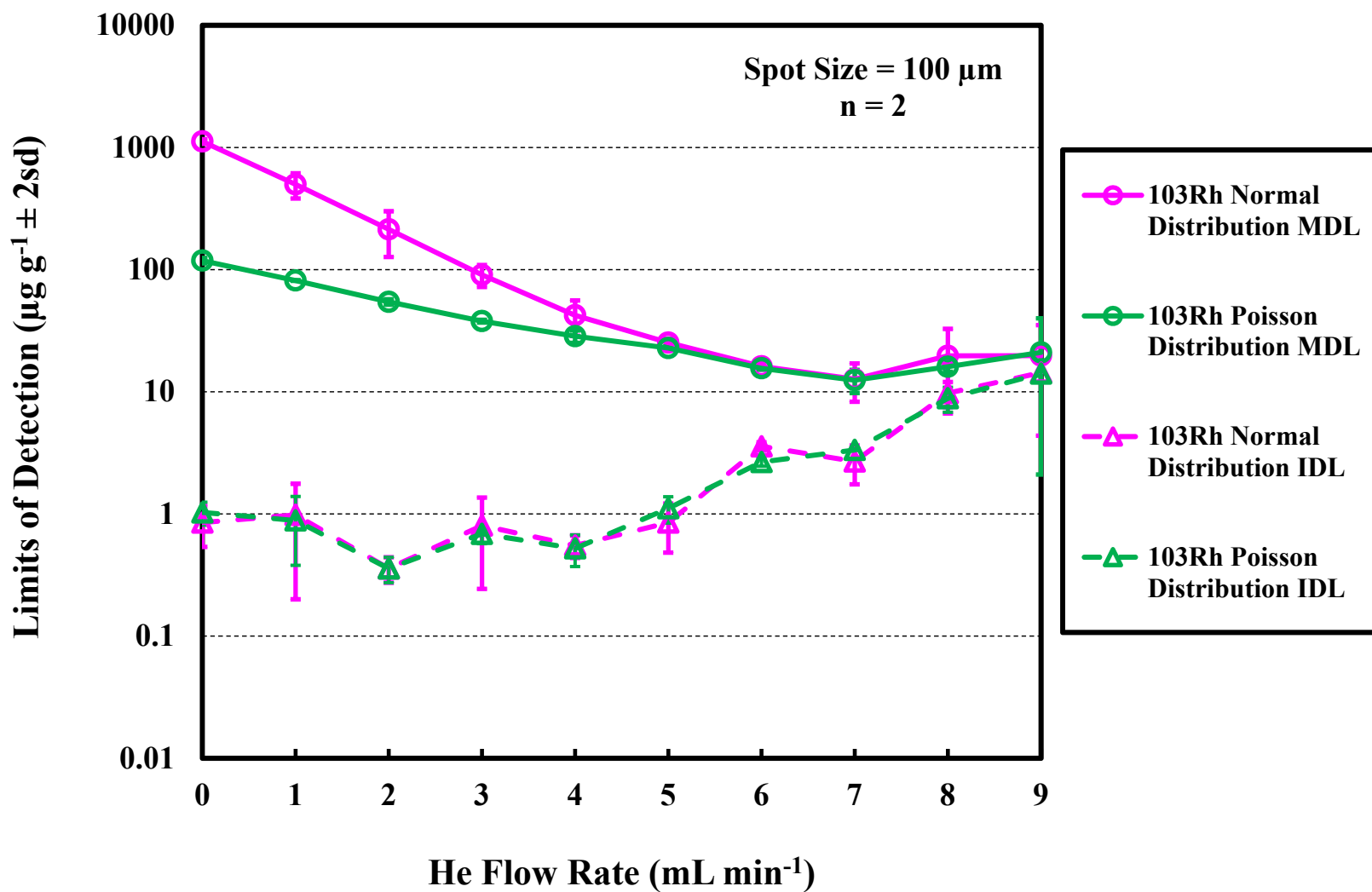
5

6 Supplementary Fig. 2-1† Method and instrument limits of detection (MLOD and ILOD) for ^{103}Rh determined using the equations of
7 Longerich et al. (1996)⁶² (normal distribution) and Pettke et al. (2012)⁶⁴ (Poisson distribution) for Agilent 7700x LA-ICP-MS analysis of
8 chalcopyrite CRG-1902 (34.52% Cu).



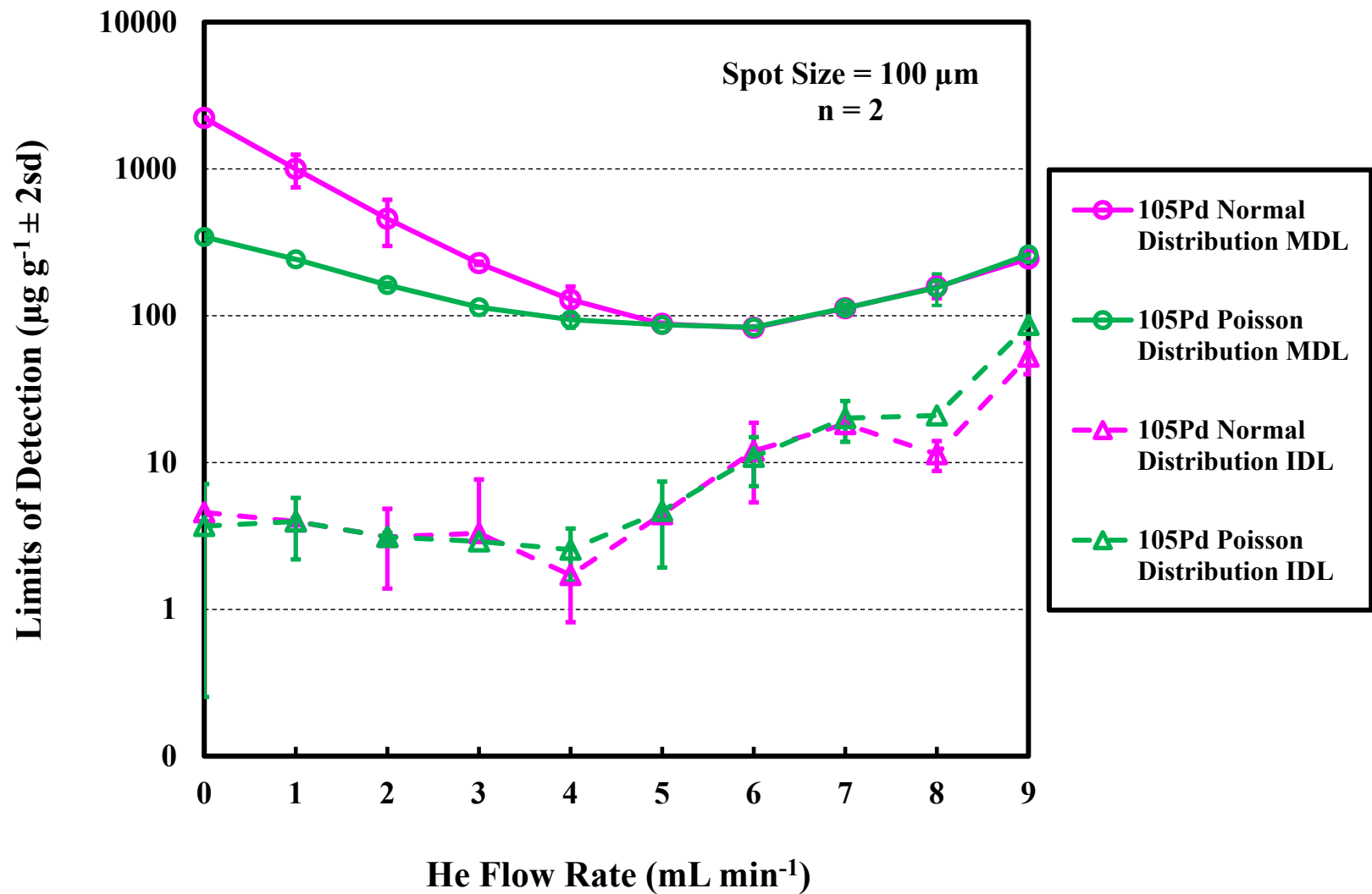
9

10 Supplementary Fig. 2-2† Method and instrument limits of detection (MLOD and ILOD) for ^{105}Pd determined using the equations of
11 Longerich et al. (1996)⁶² (normal distribution) and Pettke et al. (2012)⁶⁴ (Poisson distribution) for Agilent 7700x LA-ICP-MS analysis of
12 chalcopyrite CRG-1902 (34.52% Cu).



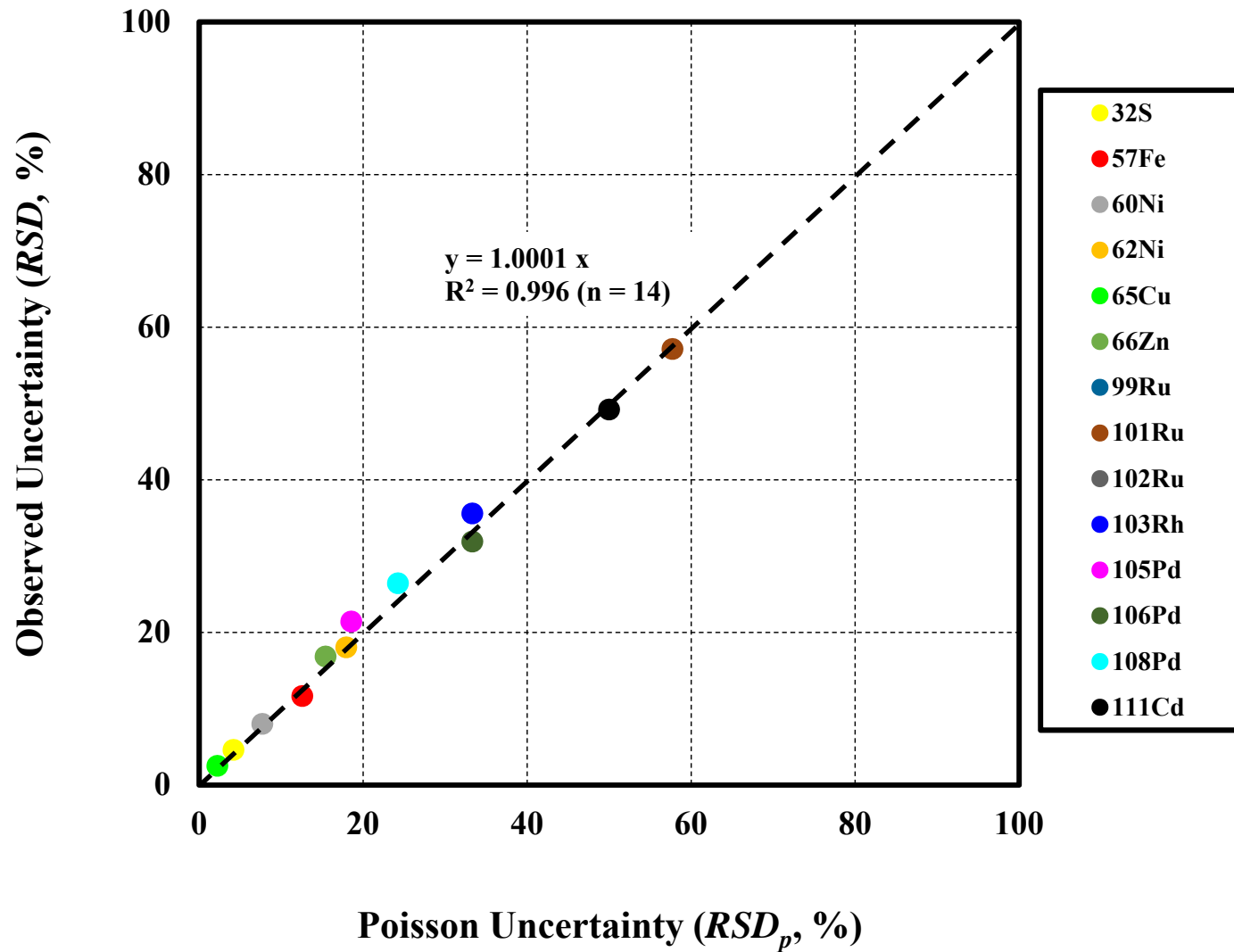
13

14 Supplementary Fig. 3-1† Method and instrument limits of detection (MLOD and ILOD) for ^{103}Rh determined using the equations of
 15 Longerich et al. (1996)⁶² (normal distribution) and Pettke et al. (2012)⁶⁴ (Poisson distribution) for Agilent 7700x LA-ICP-MS analysis of
 16 bornite OSP9 (62.19% Cu).



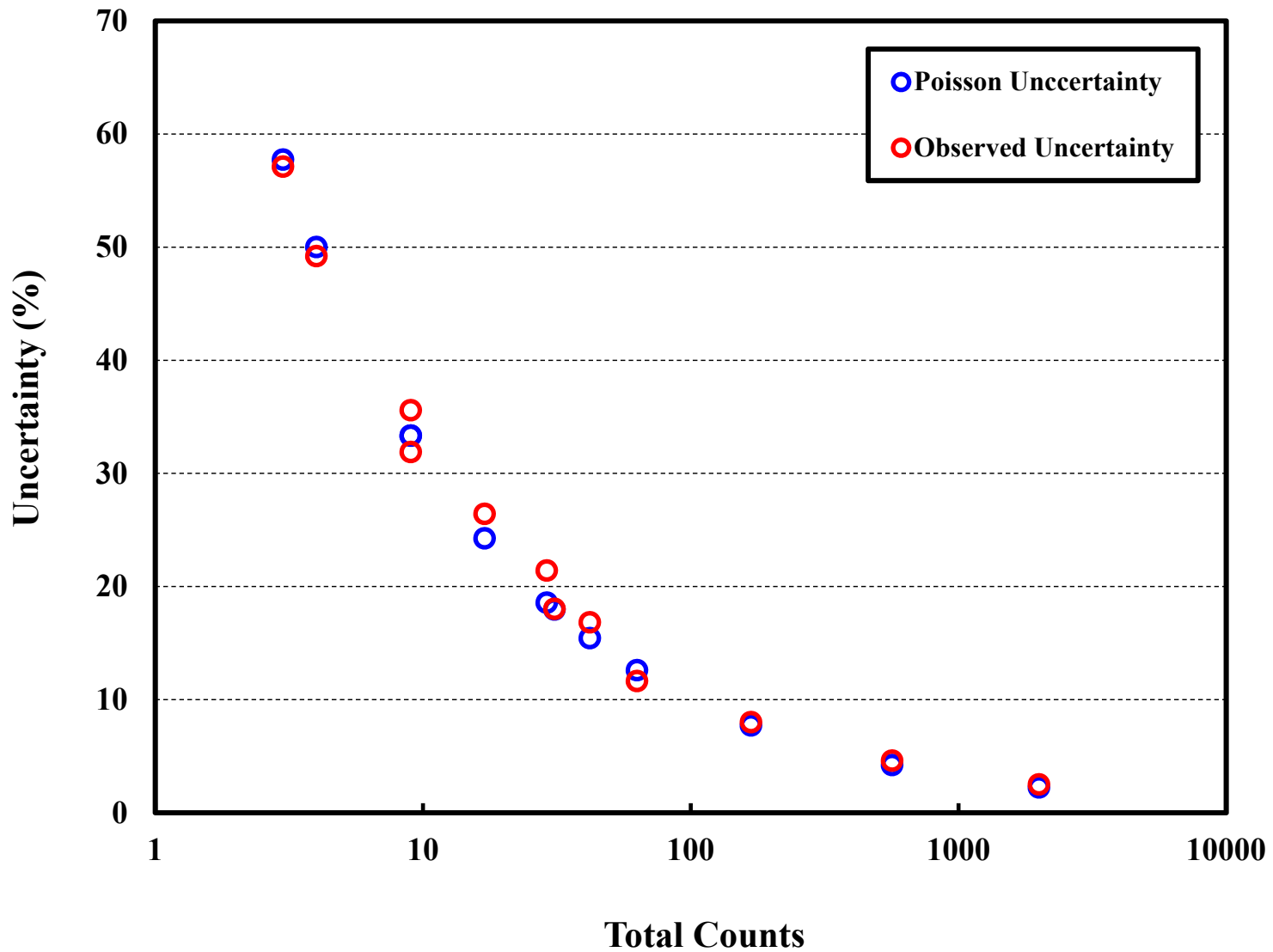
17

18 Supplementary Fig. 3-2† Method and instrument limits of detection (MLOD and ILOD) for ^{105}Pd determined using the equations of
 19 Longerich et al. (1996)⁶² (normal distribution) and Pettke et al. (2012)⁶⁴ (Poisson distribution) for Agilent 7700x LA-ICP-MS analysis of
 20 bornite OSP9 (62.19% Cu).



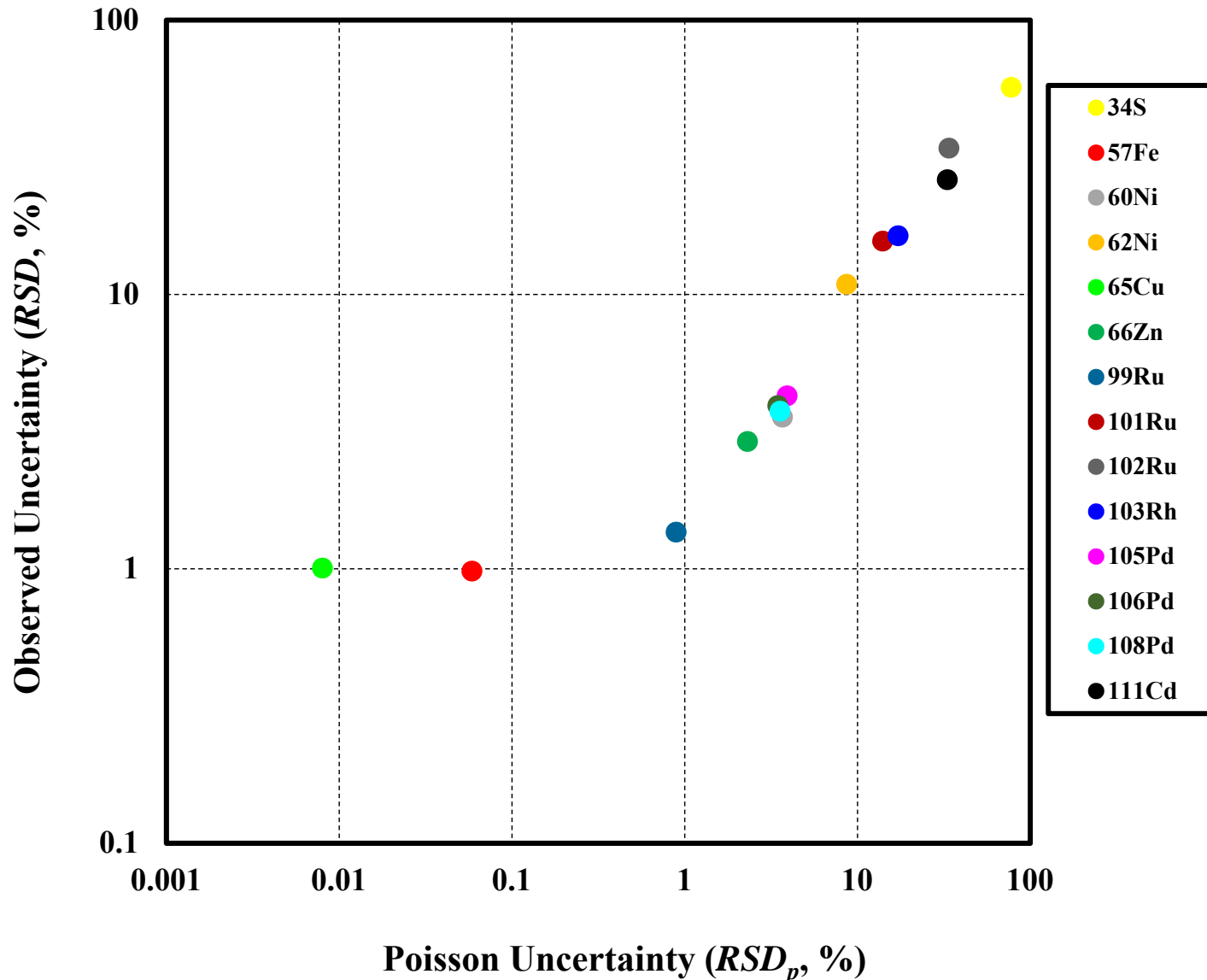
21

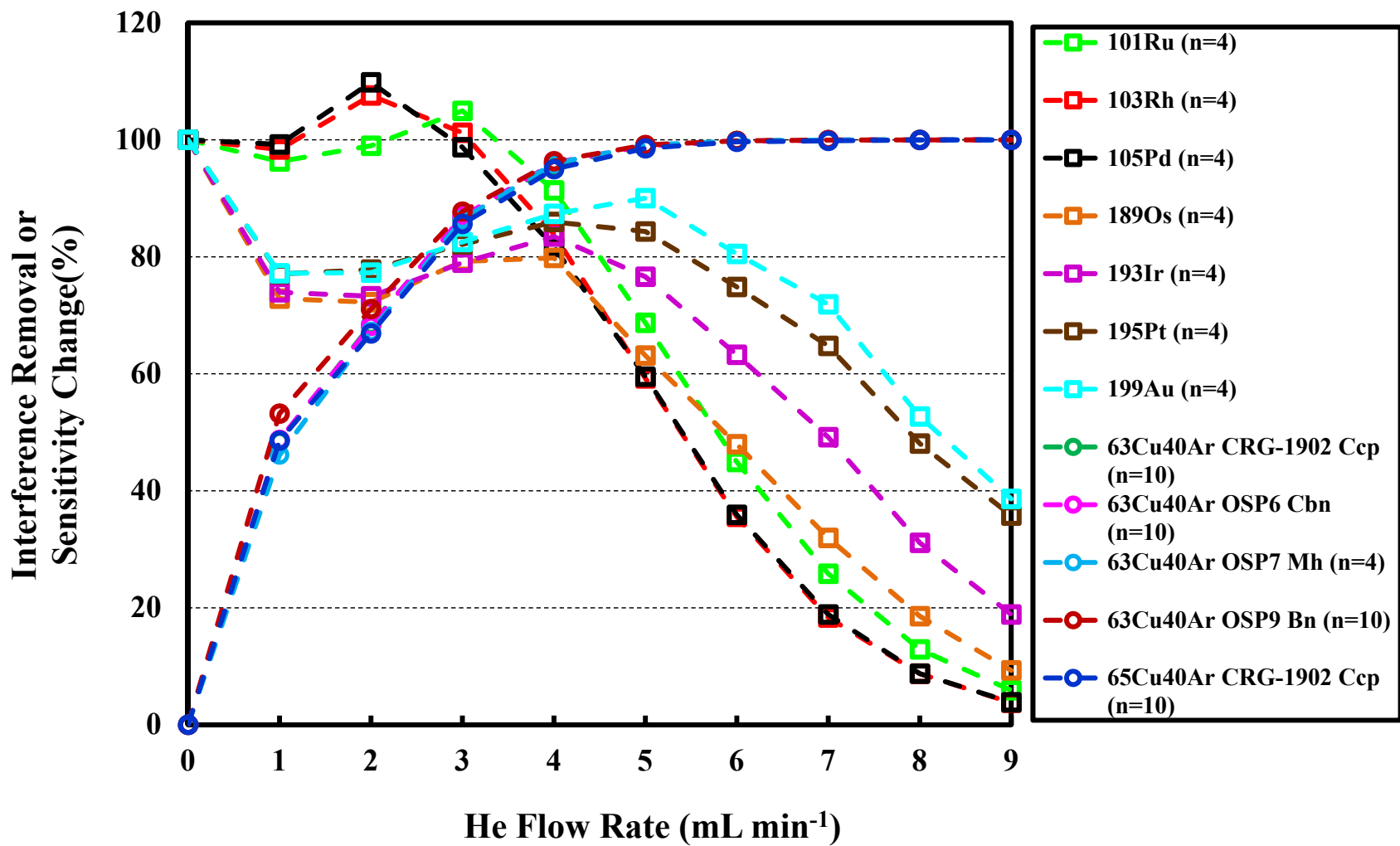
22 Supplementary Fig. 4-1† Observed uncertainty versus Poisson uncertainty for gas blank signals for 8900x LA-ICP-MS/MS PGE analysis
 23 of Cu-rich mineral bornite OSP9 (AU21A17 experiment).



24

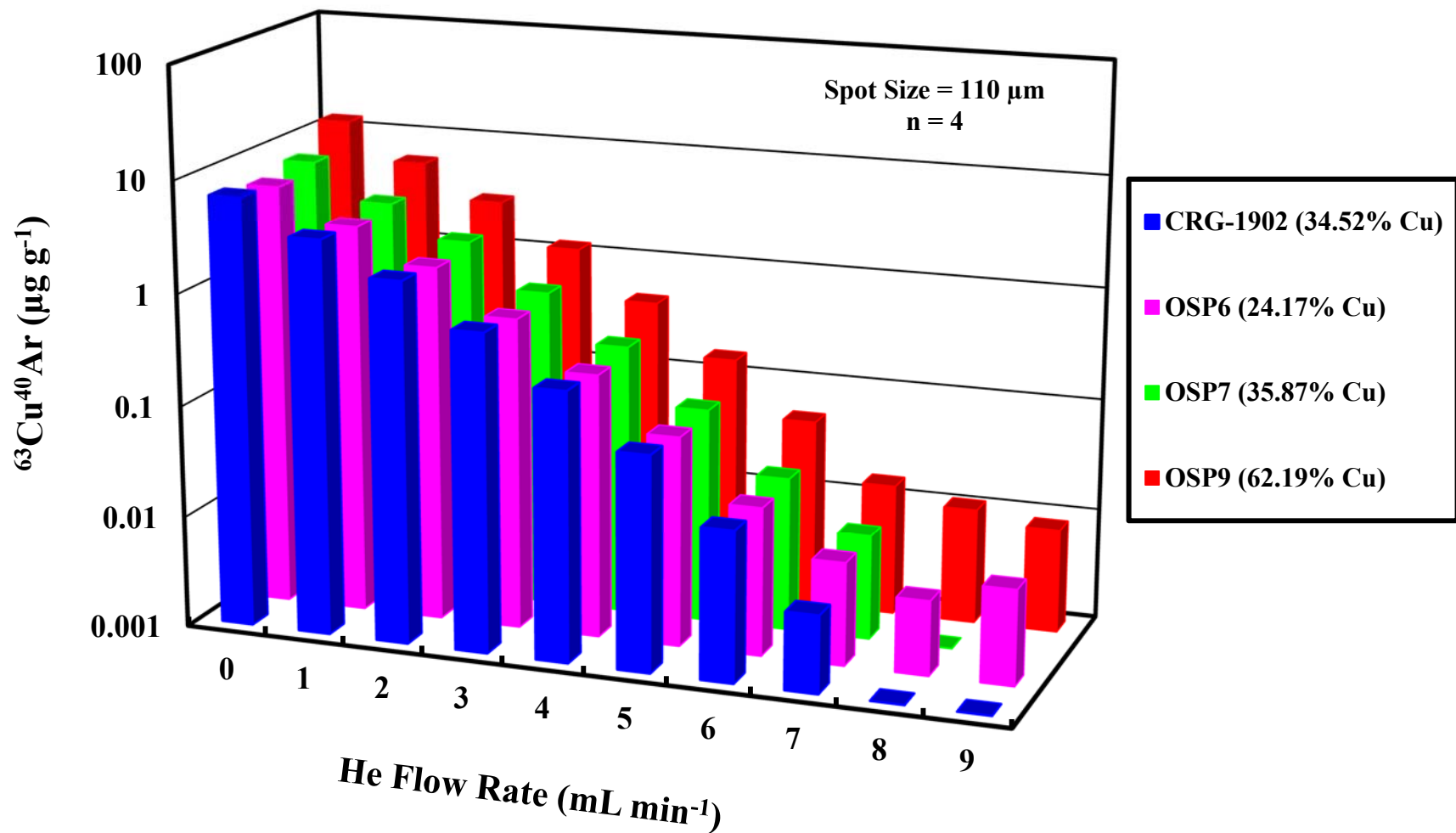
25 Supplementary Fig. 4-2† Poisson and observed measurement uncertainties versus total counts for the gas blank signals in 8900x LA-ICP-
26 MS/MS PGE analysis of Cu-rich mineral bornite (AU21A17 experiment).





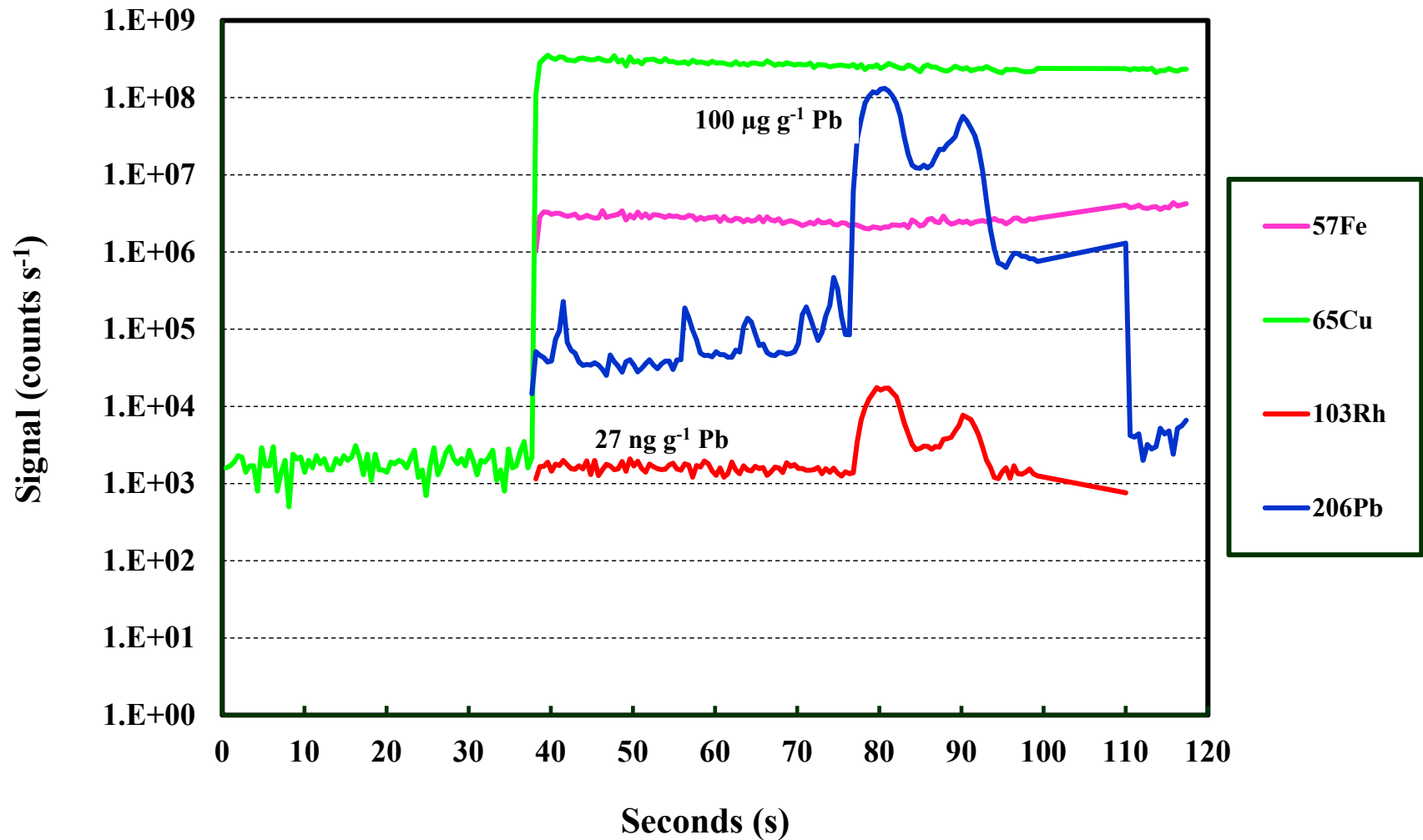
30

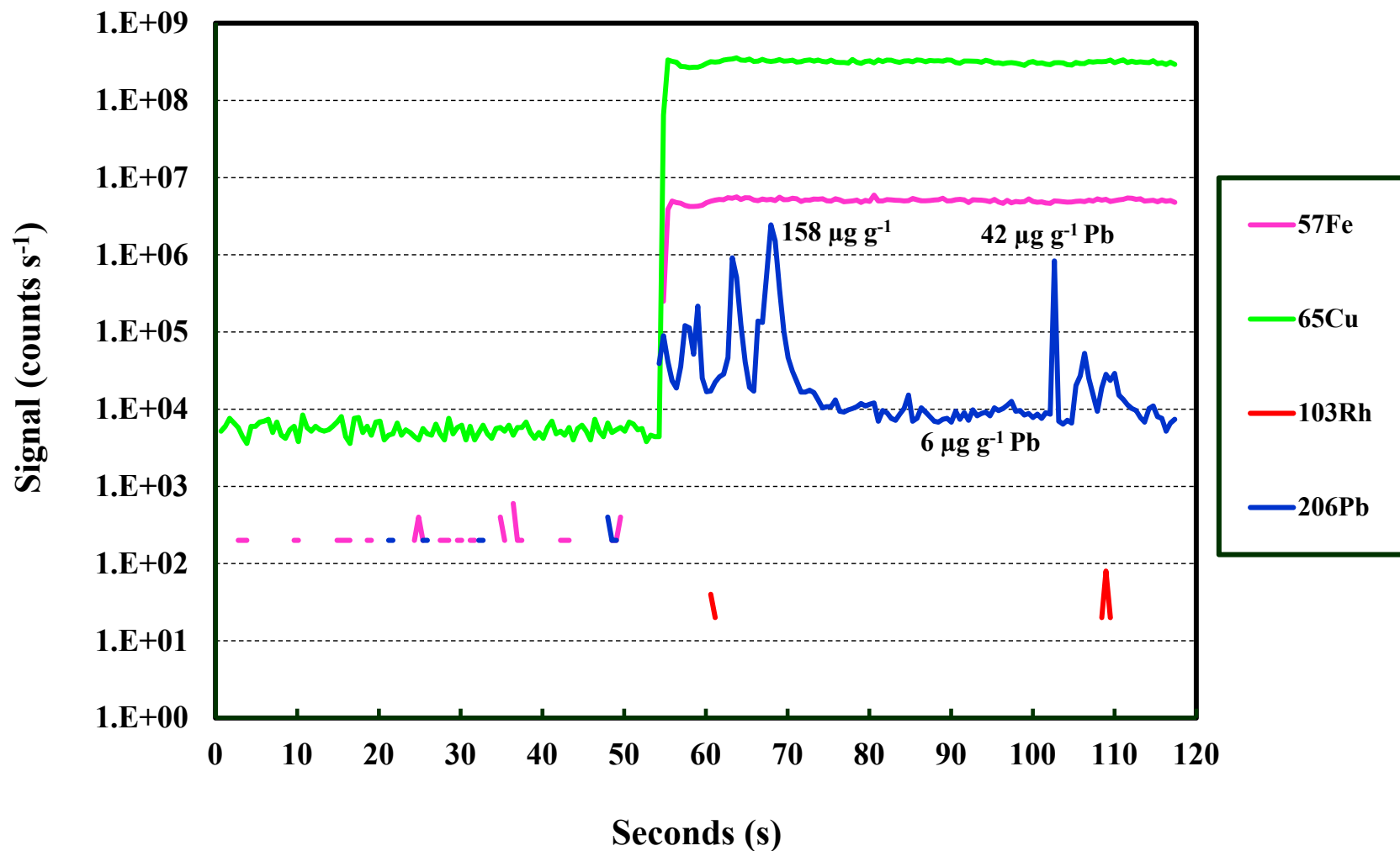
31 Supplementary Fig. 6-1† $^{63}\text{Cu}^{40}\text{Ar}^+$ and $^{65}\text{Cu}^{40}\text{Ar}^+$ interference removal and sensitivity change of $^{103}\text{Rh}^+$ and $^{105}\text{Pd}^+$, as well as other PGE,
32 with change of He collision gas flow rate using 7700x LA-ICP-MS.

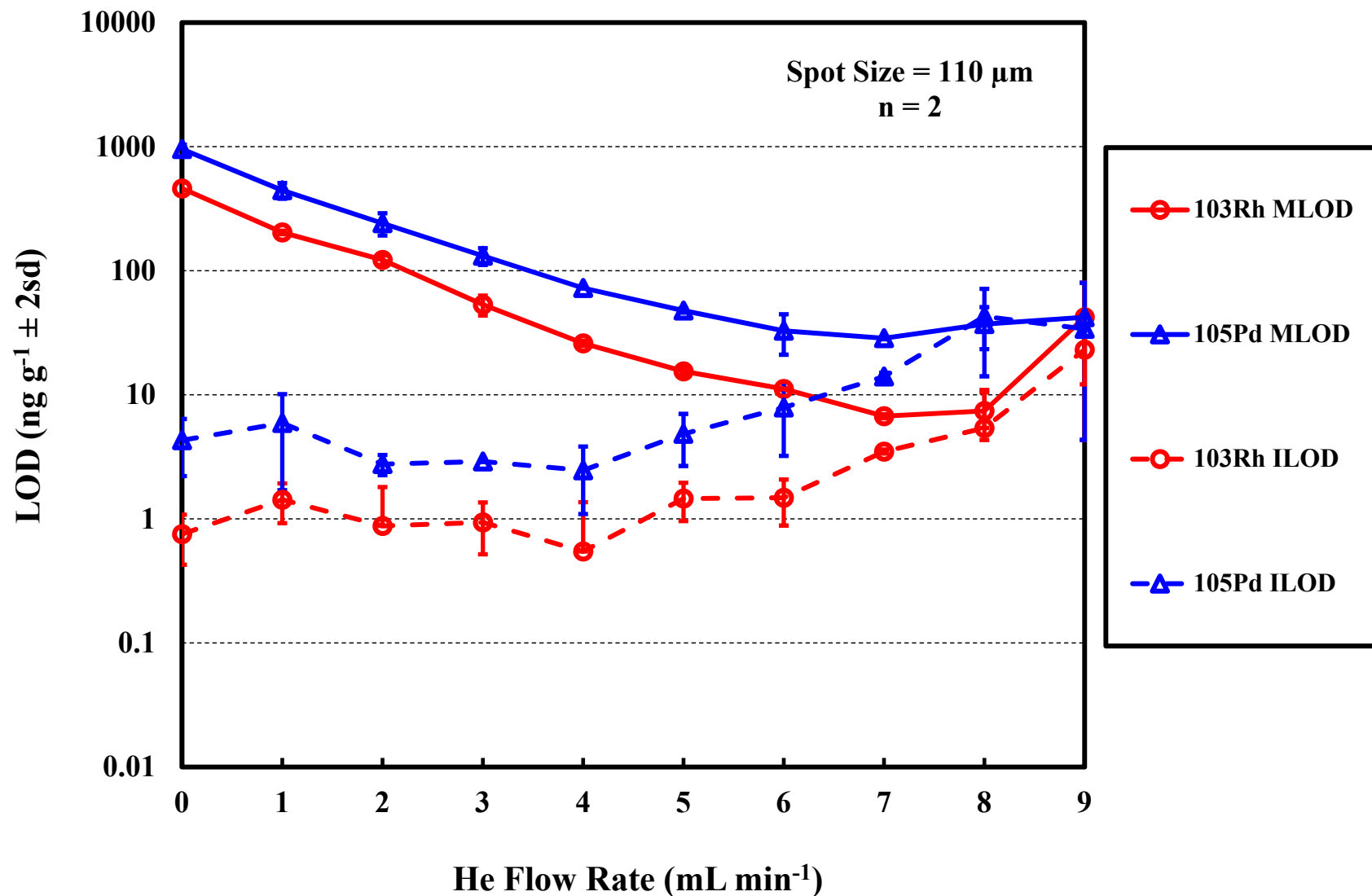


33

34 Supplementary Fig. 6-2† $^{63}\text{Cu}^{40}\text{Ar}^+$ contribution on $^{103}\text{Rh}^+$ in 7700x LA-ICP-MS analysis of Cu-rich materials with He collision gas flow
 35 rates of 0 to 9 mL min^{-1} .

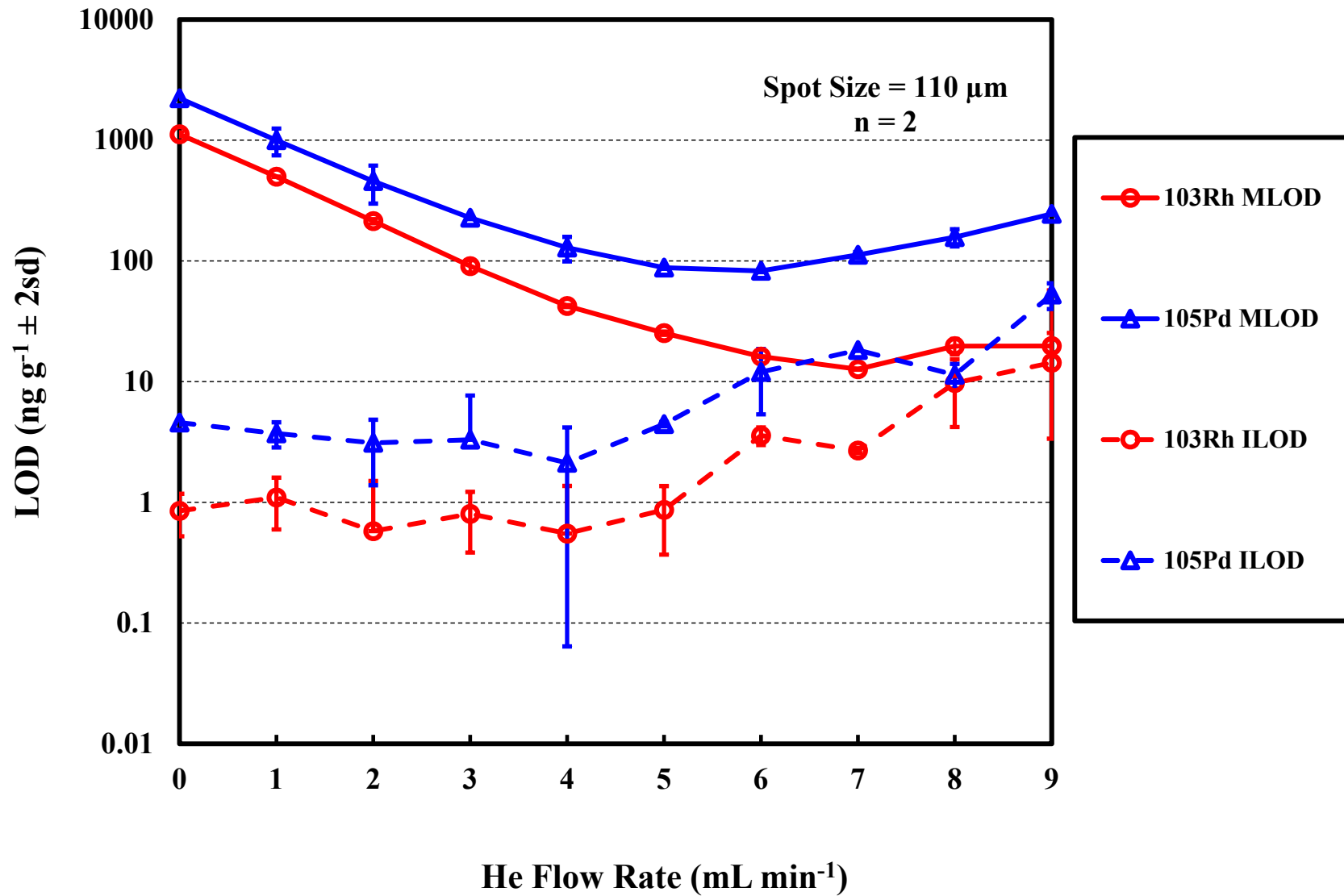






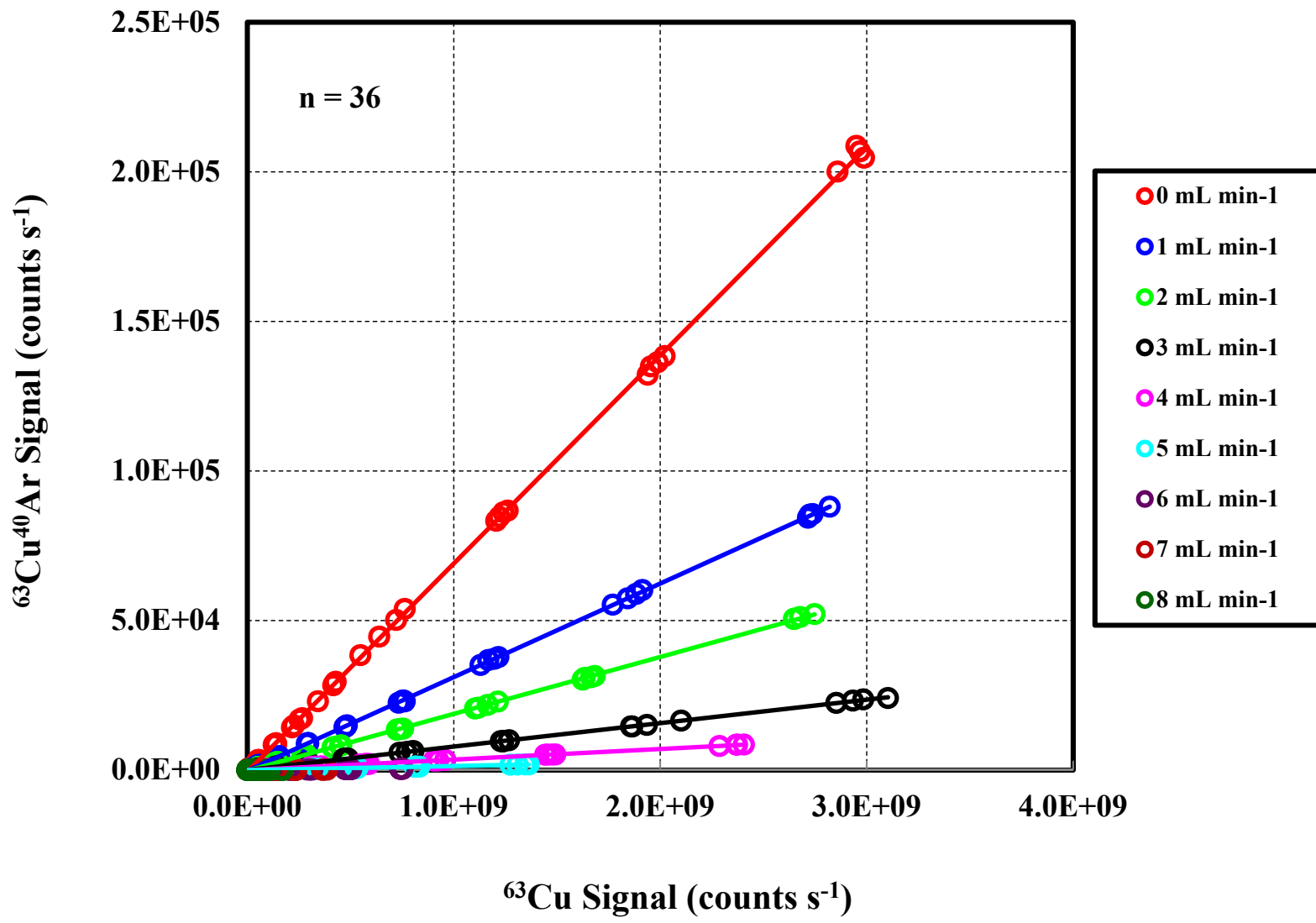
42

43 Supplementary Fig. 8-1† Method and instrument limits of detection (MLOD and ILOD) for ^{103}Rh and ^{105}Pd for Agilent 7700x LA-ICP-MS
44 analysis of chalcopyrite CRG-1902 (34.52% Cu).



45

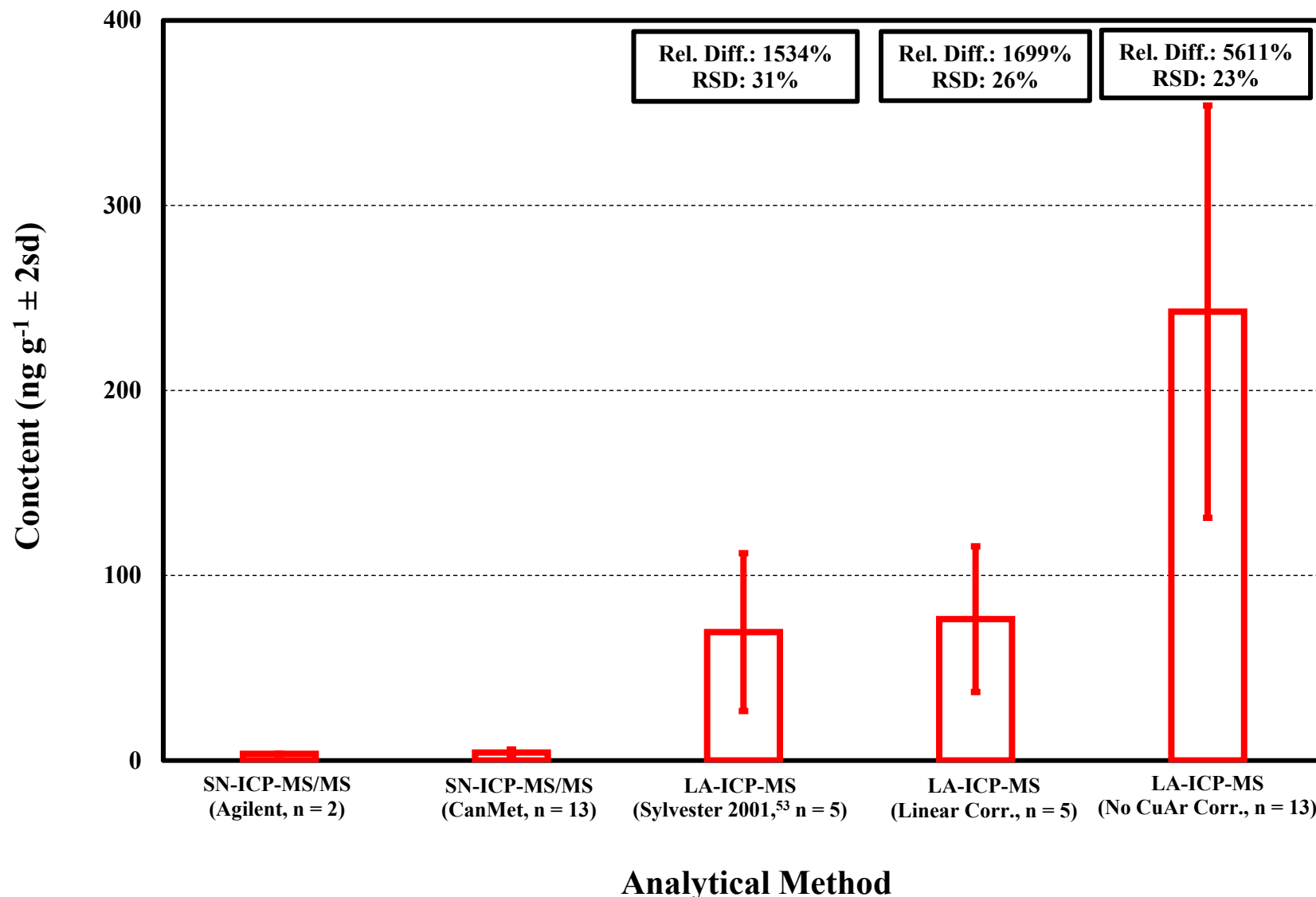
46 Supplementary Fig. 8-2† Method and instrument limits of detection (MLOD and ILOD) for ^{103}Rh and ^{105}Pd for Agilent 7700x LA-ICP-
47 MS analysis of bornite OSP9 (62.19%).



48

49 Supplementary Fig. 9† Signals (counts s⁻¹) of $^{63}\text{Cu}^{40}\text{Ar}^+$ vs. $^{63}\text{Cu}^+$ in 7700x LA-ICP-MS analyses of chalcopyrite CRG-1902 (34.52% Cu)

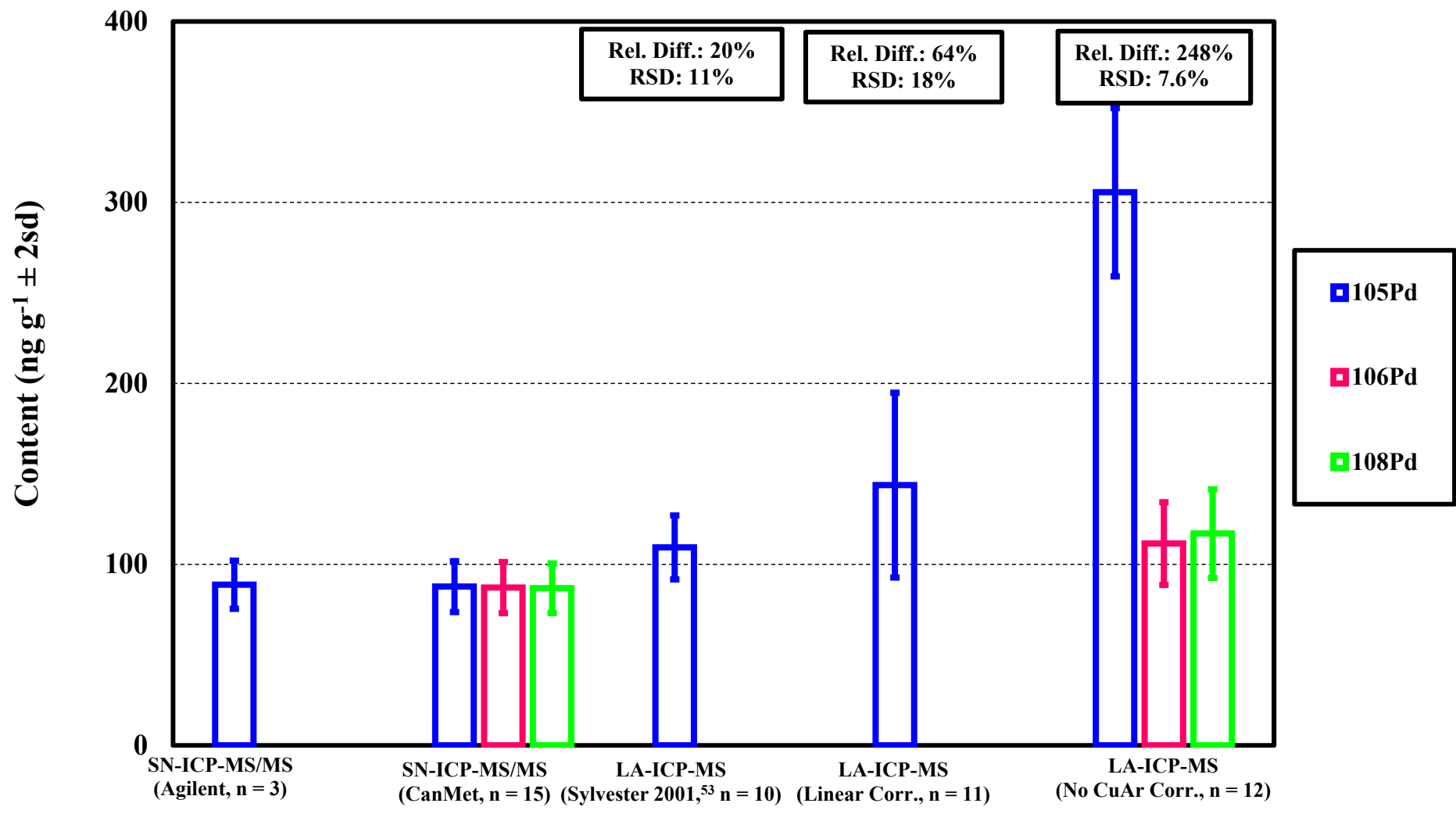
50 at He collision gas flow rate of 0 to 8 m^L min⁻¹.



51

52 Supplementary Fig. 10-1† Rh content determination with and without using the Sylvester (2001)⁵³ and linear CuAr interference correction

53 procedures for 7700x LA-ICP-MS PGE analysis of bornite OSP9 (62.19% Cu).



Analytical Method

54

55 Supplementary Fig. 10-2† Pd content determination with and without the Sylvester (2001)⁵³ and linear CuAr interference correction
 56 procedures for 7700x LA-ICP-MS PGE analysis of cubanite OSP6 (24.17% Cu).